2014

A Comparative Study of Sea Level Reconstruction Techniques Using 20 Years of Satellite Altimetry Data

M. W. Strassburg

B. D. Hamlington
Old Dominion University, bhamling@odu.edu

R. R. Leben

K.-Y. Kim

Original Publication Citation

Strassburg, M.W., Hamlington, B.D., Leben, R.R., & Kim, K.Y. (2014). A comparative study of sea level reconstruction techniques using 20 years of satellite altimetry data. *Journal of Geophysical Research: Oceans, 119*(7), 4068-4082. doi: 10.1002/2014JC009893

AGU PUBLICATIONS

JGR

Journal of Geophysical Research: Oceans

RESEARCH ARTICLE

10.1002/2014JC009893

Key Points:
- Sea level reconstructions are formed with different basis function methods
- CSEOF methods are less sensitive to tide gauge distribution and high-frequency variations than EOF methods

Correspondence to:
M. W. Strassburg,
mathew.strassburg@colorado.edu

Citation:
Strassburg, M. W., B. D. Hamlington, R. R. Leben, and K.-Y. Kim (2014), A comparative study of sea level reconstruction techniques using 20 years of satellite altimetry data, *J. Geophys. Res. Oceans*, *119*, 4068–4082, doi:10.1002/2014JC009893.

Received 7 FEB 2014
Accepted 11 JUN 2014
Accepted article online 14 JUN 2014
Published online 3 JUL 2014

A comparative study of sea level reconstruction techniques using 20 years of satellite altimetry data

M. W. Strassburg[1], B. D. Hamlington[2], R. R. Leben[1], and K.-Y. Kim[3]

[1]Colorado Center for Astrodynamics Research, University of Colorado, Boulder, Colorado, USA, [2]Cooperative Institute for Research in Environmental Sciences, University of Colorado, Boulder, Colorado, USA, [3]School of Earth and Environmental Science, Seoul National University, Seoul, South Korea

Abstract Sea level reconstructions extend spatially dense data sets, such as those from satellite altimetry, by decomposing the data set into basis functions and fitting those functions to in situ tide gauge measurements with a longer temporal record. We compare and evaluate two methods for reconstructing sea level through an idealized study. The compared sea level reconstruction methods differ in the technique for calculating basis functions, i.e., empirical orthogonal functions (EOFs) versus cyclostationary EOFs (CSEOFs). Reconstructions are created using Archiving, Validation, and Interpretation of Satellite Oceanographic (AVISO) satellite altimetry data and synthetic tide gauges. Synthetic tide gauge records are simulated using historical distributions and real high-frequency signal to test reconstruction skill. The CSEOF reconstructions show high skill in reproducing variations in global mean sea level (GMSL) and ocean climate indices, and are affected less by both limited tide gauge distribution and added high-frequency tide gauge signal than EOF reconstructions. Typically, CSEOF reconstructions slightly underestimate sea level amplitudes while EOF reconstructions overestimate sea level amplitudes, in some cases, significantly. Both of these results are accentuated with decreasing quality of the synthetic tide gauge data set. Additionally, we investigate how the reconstructions differ when reconstructing with more of the variance retained in the basis functions. Increasing the variance explained by the basis functions from 70% to 90% reduces the efficacy of an EOF reconstruction to reproduce common ocean indices when noise is included in the tide gauge data sets. These results show that in the idealized comparative cases examined the CSEOF method of sea level reconstruction creates more robust reconstructions, especially when less than ideal tide gauge data are used.

1. Introduction

The 20 year sea level record from satellite altimetry has greatly advanced understanding of oceanic processes and their impact on climate. Satellites such as TOPEX/Poseidon and the Jason series provide nearly global sampling of sea level every 10 days, allowing for scientific analysis of topics ranging from mesoscale circulation to the rate of sea level rise. Unfortunately, altimetry data of sufficient accuracy for climate studies are nonexistent before the early 1990s, when TOPEX/Poseidon became operational. Prior to this, the only means of measuring sea level was through tide gauges. Tide gauges are distributed on coastlines around the world with some records dating back to the 1800s. Most records, however, begin in the 1950s or later. The usefulness of tide gauge data is limited due to geographic clustering, a scarce number of gauges, and a lack of gauges in the middle of the ocean basins. Sea level reconstructions offer a solution to these shortcomings by decomposing the globally complete satellite altimetry data set into basis functions and fitting those functions to the long records of the tide gauges. This yields a data set with the high spatial resolution of satellite altimetry and the longer record length of tide gauges.

Reconstructing sea level initially focused on global mean sea level (GMSL) rise preceding the satellite altimetry record [e.g., *Church et al*., 2004, hereinafter *CW2004*; *Hamlington et al*., 2011, hereinafter *H2011*]. It has since been determined that sea level reconstructions can also provide valuable insight into other ocean signals prior to the satellite altimetry era [e.g., *Hamlington et al*., 2013]. Of particular interest are longer period signals and the modulation of shorter signals, as these could not have been fully captured in the short 20 year satellite altimetry record. Combining a shorter but essentially complete global data set, such as one offered by satellite altimetry, with the longer but sparsely distributed tide gauge data set draws on the advantages of both data types, allowing for better monitoring and understanding of sea level signals associated with observed oceanic processes and greater predictive capabilities of what is to come. Sea level

reconstructions can also be used to explain secular trends and multiyear climate variability such as the El Niño-Southern Oscillation (ENSO), as shown in *H2011*. More recently, reconstructions have proven useful in capturing lower-frequency variability, such as the contribution of the Pacific Decadal Oscillation (PDO) to GMSL [*Hamlington et al*., 2013].

The most accepted approach for sea level reconstructions is similar to that used by *Smith et al*. [1996], *Kaplan et al*. [1998], and *Smith and Reynolds* [2004] for sea surface temperature (SST), and *Chambers et al*. [2002], *CW2004*, *Berge-Nguyen et al*. [2008], *Llovel et al*. [2009], *Church and White* [2011], *Ray and Douglas* [2011], and *Meyssignac et al*. [2012] for sea level. It involves forming a set of basis functions through empirical orthogonal function (EOF) decomposition of the dense training data set. This training data set can be either satellite altimetry data, as used here, or general ocean circulation models. The former has the benefit of using actual, remotely sensed sea level, while the latter has a longer time span to better fit the tide gauges. A second technique uses a basis function decomposition process known as cyclostationary empirical orthogonal function (CSEOF) analysis, proposed by *Kim et al*. [1996], and verified by *Kim and Wu* [1999], among others. The CSEOF technique excels in extracting physical climate modes from geophysical data sets and was adopted and implemented by *Hamlington et al*. [2011, 2012, 2013] for sea level reconstruction. Basis functions found using either of the above methods are then used to interpolate the tide gauge data to create a reconstruction.

Although the method for computing basis functions varies between EOF and CSEOF reconstructions, they are similar in that they decompose the data into spatial patterns (known as loading vectors (LVs)) with a corresponding amplitude time series (known as the principal component (PCs) time series). The distinguishing difference is that CSEOFs can account for nonstationary signals because each LV is not a single spatial pattern, but a set of time-dependent spatial patterns corresponding to a nested period. Each individual LV and PC time series pair represents a mode of variability, and summing over all modes recovers the initial data set. The lower-order modes explain more variance and higher-order modes contain more of the noise inherently found in the initial data set. To avoid reproducing this noise in the reconstruction, only a limited number of lower-order modes are used in a reconstruction. The signal neglected in the higher-order modes is referred to as truncation error. There is a delicate trade-off when selecting the number of modes to use: keeping less variance causes physical signals to be left out of the reconstruction, while keeping too much variance may cause increased noise levels in the reconstruction.

While overcoming some of the issues associated with short record lengths and sparse data, sea level reconstructions are still limited by data availability. Capturing variability on time scales much longer than the training period is questionable, and small-scale regional variability is unlikely to be explained well in the reconstruction due to the poor spatial coverage of the historical data. Recent studies have shown that the regional patterns of sea level variability seen in the training data sets used to find the basis for reconstruction change on much longer time scales than the calibration period [*Calafat et al*., 2014; *Chambers et al*., 2012]. *Llovel et al*. [2009] and *Meyssignac et al*. [2012] attempted to use model data sets to allow for longer calibration periods, which is a promising method if the model data set is assumed to be correct. Furthermore, as discussed by *Calafat et al*. [2014], the tide gauges are not always representative or correlated with the nearby open ocean they are being used to reconstruct. It is important to keep in mind that while certain things can be done to improve sea level reconstructions, the resulting data product is still hampered by data availability issues.

Whether either basis function technique has specific benefits or limitations with regards to sea level reconstruction is still an active area of research and there is currently a lack of literature on the subject. The use of sea level reconstructions is growing because of the advantages of a longer reconstructed sea level record for the study of climate, which creates a need to optimize and validate the reconstruction technique. To date, only two noteworthy sea level reconstruction comparisons have been published, both dealing strictly with the EOF technique [*Christiansen et al*., 2010; *Calafat et al*., 2014]. In this paper, we investigate two different methods for calculating basis functions while reconstructing the 20 year satellite altimetry record in an idealized, experimental setting to expand on previous reconstruction comparison work. Initially, basis functions using both EOF and CSEOF decomposition techniques are calculated from the complete satellite altimetry training data set. Synthetic tide gauge data are interpolated by the basis functions over the training time period (i.e., from 1993 to present). Synthetic tide gauge data are the time series from a single spatial grid point in the satellite altimetry data set at locations akin to actual tide gauges. Reconstructing using

synthetic tide gauges and over the calibration time period allows for an ideal comparison to truth, in which the only variables are reconstruction technique and the number and quality of tide gauges used. While the reconstructions considered here are not necessarily realistic and keeping in mind the conclusions from studies like that of [*Calafat et al*., 2014], creating a control experiment like the one in this study provides results and comparisons that can help inform us on how to best create reconstructions using real tide gauges.

At the core, this research compares the two methods of calculating basis functions that are currently used for sea level reconstructions. This comparative study seeks to answer three open questions in an idealized setting using the available satellite altimetry record:

1. How sensitive is each method to tide gauge selection?

2. How sensitive is each method to high-frequency tide gauge variability?

3. How does the amount of reconstructed variance affect reconstruction quality?

To answer these questions, CSEOF and EOF reconstructions are created with varying tide gauge distribution based on historical completeness (section 3), with tide gauge time series that include noise (section 4), and with basis functions consisting of different percentages of retained variance (section 5). These reconstructions are then compared with the original data set by investigating regional trends, point-wise correlation, point-wise relative amplitude, reproducibility of variability in GMSL, and reproducibility of known oceanographic indices. Section 6 focuses on summary discussions, conclusions, and future avenues of research regarding this topic.

2. Data and Methods

2.1. Satellite Altimetry Data Set

The basis of estimation for the reconstructions and the benchmark with which we compare is the Archiving, Validation, and Interpretation of Satellite Oceanographic (AVISO) half degree gridded data set spanning 1993 to 2012 created from TOPEX/Poseidon, Geosat Follow-On, GFO, ERS-1 & 2, Jason-1 & 2, and Cryosat-2 satellite altimetry measurements. The Ssalto/Duacs multimission altimeter data processing system created the data set using improved homogeneous corrections, global crossover minimization, and intercalibration to derive highly accurate along-track anomaly data. Glacial isostatic adjustment (GIA) corrections were not applied for this analysis. The along-track data were gridded using space-time objective mapping to account for correlated noise [*Le Traon et al*., 1998]. This data set was updated, reprocessed, and released in June 2013. In this study, weekly data on a $0.5^\circ \times 0.5^\circ$ grid, spanning from 1993 to 2012 are used, which is subsampled from the original $0.25^\circ \times 0.25^\circ$ gridded AVISO data set. For use as the training (or calibration) data, each grid point time series had a mean, and linear, annual period, and semiannual period least squares fits removed. Any grid points that were not continuous over the entire time period were removed.

The seasonal cycle is a dominant source of periodic variability in ocean height but is not generally a focus of sea level reconstructions and has little scientific interest in studies of long-term variability. Thus, we do not consider it here. Leaving a secular trend in the training data set complicates the reconstruction process using both methods of basis function calculation. The linear trend is not decomposed into a single mode because of the limited satellite data record length. For these reasons and because reconstructing secular trends in GMSL has previously been discussed [*Christiansen et al*., 2010; *Calafat et al*., 2014], we choose to exclude this signal from the training data set. While removing the secular trend in the training data does not allow the reconstruction to capture long-term trends in GMSL, it is still able to capture regional trend patterns due to the trend remaining in the synthetic tide gauges. The zero-mean trend map of the AVISO data set is shown in Figure 1.

2.2. Synthetic Tide Gauge Data Sets

Synthetic tide gauge data sets are grid points in the AVISO data set nearest to actual tide gauge locations from the Permanent Service for Mean Sea Level (PSMSL). Only revised local reference (RLR) tide gauge locations with significant record length were taken into account, which resulted in a total of 412 separate locations since 1900 (Figure 2). A more detailed discussions of tide gauge selection can be found in *CW2004* and *H2011*. As with the training data set, seasonal cycles were removed from the tide gauge data so as not

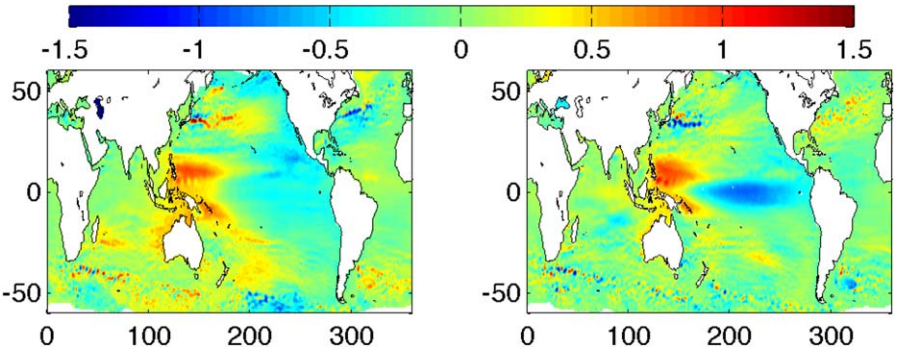

Figure 1. (left) Trend pattern from the 1993–2012 AVISO record. (right) Trend pattern from the 1993–2009 *H2011* CSEOF reconstruction record. An average spatial trend of 0.26 and 0.28 has been removed from each map, respectively. All units in cm/yr.

to reproduce well resolved annual and semiannual signals. However, unlike the training data set, linear trend signals are retained allowing the reconstructions to capture regional trends.

Reconstructions were created using all 412 synthetic tide gauges, as well as with subsets of tide gauges at decadal intervals. To look at the effects of using different tide gauge distributions, subsets were taken from each decade from 1900 onward. If a tide gauge produced data for a majority of a decade, then the corresponding grid point became a synthetic gauge for that decade's subset. As can be seen in Figure 2, the number of available in situ measurements through tide gauges varies significantly over the past century, with fewer than 100 stations prior to 1940 and more than 300 in the 1990s.

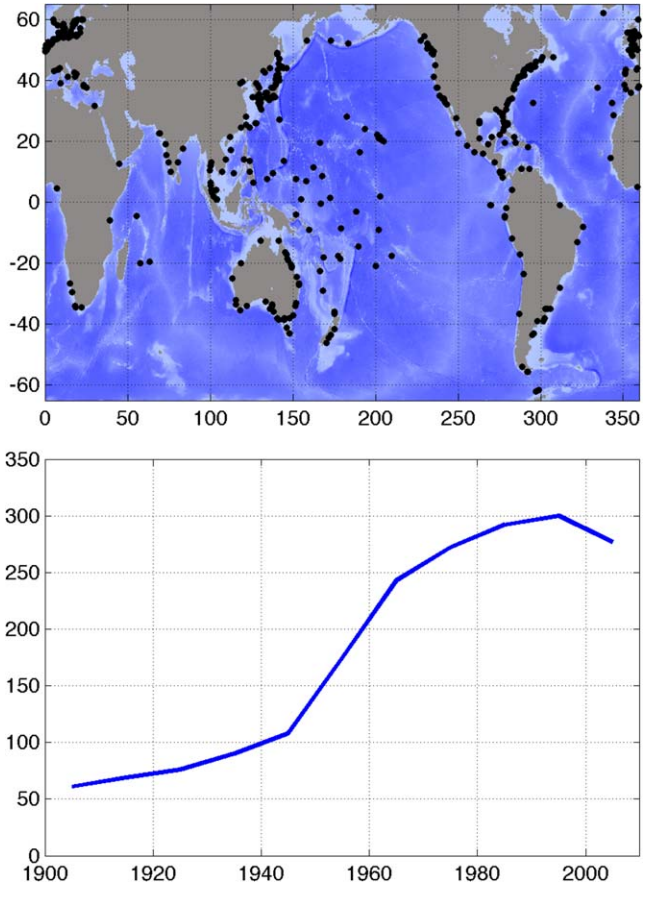

Figure 2. (top) Spatial distribution of all tide gauges used and (bottom) number of available tide gauges during a given decade.

Additionally, to investigate more realistic tide gauge time series, high-frequency variability was added to the synthetic tide gauge data set. This signal was estimated by removing the mean of the monthly tide gauge measurements and performing a 3 month high-pass filter. This was found by removing a 3 month running mean from the tide gauge data, and resulted in a zero-mean signal with an average standard deviation of 2.8 cm. These high-frequency time series were then randomly shifted and added to the synthetic tide gauge time series. The magnitude of this signal agrees well with that used by *van Onselen* [2000] to create simulated tide gauge signals in a study of the effects of tide gauge data quality on detecting sea level height variations.

2.3. EOF Versus CSEOF

2.3.1. Basis Functions

The two basis function methods to be compared are EOF and CSEOF. Although both have

similarities in the structure of the final LVs and PCs, the technique used to decompose the initial data set is quite different. A summary of each method is given below.

2.3.1.1. EOF Reconstructions

Singular value decomposition (SVD) is used to calculate the eigenvectors and eigenvalues of the spatial covariance structure, as explained in *CW2004* and *Meyssignac et al*. [2012]; the reader is referred to consult their work for a more in-depth description of the process. An initial data set, H, can be broken down into spatial eigenvectors also called loading vectors (LVs), and amplitude time series also called principal component (PC) time series.

$$H(r,t)=LV(r)PC(t) \tag{1}$$

Each EOF mode is comprised of a spatial pattern (LV) modulated by a corresponding amplitude time series (PC). The first few grave modes contain the most explained variance and often depict physical phenomena. For reconstruction of sea level prior to the timespan of the original data, amplitude time series (PC^{α}s) are calculated based on how the tide gauges fit the satellite data. These coefficients are found by solving for least squares or minimizing a cost function [see a comparison in *Christiansen et al*., 2010]. For the work shown here, a 1 cm observational error in the cost function was used. An alternate observational error may improve reconstruction skill, particularly in the case of the EOF reconstruction, but for the sake of comparison, only a consistent value across techniques is required. A value of 1 cm lies in between the error values selected in *CW2004* and *Calafat et al*. [2014]. The reconstruction, $\hat{H}$, can then be formed in the following manner:

$$\hat{H}(r,t)=\sum_{i=1}^{K} LV_i(r)PC_i^{\alpha}(t) \tag{2}$$

In equation (2), K is the total number of modes used to create the reconstruction. As explained by *H2011*, EOF basis functions may not be ideal for sea level reconstruction because the LVs are forced to be stationary with respect to time (no time dependence). That is, a certain mode can contribute more or less to the reconstructed data set from a temporal standpoint but the spatial pattern is fixed. This limits EOF reconstruction's ability to extract cyclostationary signals such as propagating waves or moving periodic patterns (e.g., *H2011*).

This analysis was initially performed with and without using an EOF0. *CW2004* added a homogeneous EOF (known as EOF0, or mode of 1s) with unit amplitude prior to fitting to the tide gauges to account for ocean mass and volume variations causing mean sea level changes. This allows for most of the secular trend to be extracted in one mode, but constrains the entire reconstruction period to a similar trend. *Calafat et al*. [2014] showed that when EOF0 is included, the reconstructions ability to capture variability diminishes because the method removes the global mean information from each individual mode. We also found that including EOF0 decreases all aspects of reconstruction quality with the exception of GMSL trend. Because secular trends in global sea level are not considered in this work, no results from reconstructions including a mode of 1s are included.

2.3.1.2. CSEOF Reconstructions

CSEOF analysis was first introduced by *Kim et al*. [1996] as a method to extract time-varying climate signals in the climate and have been shown to surpass EOFs in capturing cyclostationary signals [*Kim and Wu*, 1999]. Simply stated, the difference between EOFs and CSEOFs is the ability for CSEOFs to capture spatial patterns that vary in time and space. This is possible because the spatial maps comprising the CSEOF LVs are time dependent, whereas EOF LVs are only varying spatially. The details for CSEOF analysis are complex; however, they are unnecessary for the understanding of this comparative study. CSEOF analysis is briefly introduced below and the reader is directed to *Kim and North* [1997] if more detail is desired.

CSEOF LVs are periodic with a chosen "nested period," with a period of d in (3). This period is selected to best reflect the data type in question. Climate and geophysical data sets exhibit 1 year periodicity primarily due to seasonal variations in solar insolation, making a 1 year nested period a valid choice in the present study. *H2011* demonstrated that a 1 year nested period can also extract lower-frequency signals, such as the El Niño Southern Oscillation (ENSO) signal, which has a 3–6 year stochastic period, and is phase locked

to the annual cycle. For more discussion, refer to *Yeo and Kim* [2013]. Therefore, depending on the frequency of the data sampling, each CSEOF LV consists of a number of spatial maps with a corresponding PC. With a 1 year nested period, there are 52 maps in each LV when considering weekly data. For a reconstruction comparable to that shown in (2), the following applies for CSEOFs:

$$\hat{H}(r,t)=\sum_{i=1}^{K} LV_i(r,t)PC_i^{\alpha}$$
$$LV(r,t)=LV_i(r,t+d) \tag{3}$$

Again, more details are available in *Kim et al*. [1996]. A trend map from the published *H2011* CSEOF reconstruction is shown in Figure 1. As can be seen, the trends generally agree with the AVISO trend map (the slight difference in the span of data is due to limited reconstruction data; the agreement improves slightly when taken over a common time period, i.e., 1993–2009).

2.4. Ocean Parameter/Index Calculations

Five different parameters are used to quantify the ability of a reconstruction to reproduce observed ocean signals. The first is latitude weighted Global Mean Sea Level (GMSL) with a mean trend of ~3.2 mm/yr removed, and the remaining four are sea surface height (SSH) equivalents of common ocean indices typically calculated by sea surface temperature (SST): Pacific Decadal Oscillation (PDO), Atlantic Multidecadal Oscillation (AMO), Niño3, and Niño4. To calculate these indices, sea level from the training or reconstruction data sets was latitude weighted and averaged in the areas associated with AMO [*Kerr*, 2000], Niño3, and Niño4 [*Stenseth et al*., 2003]. In the case of PDO, the leading principal component from sea level in the Northern Pacific PDO region is used [*Stenseth et al*., 2003; *Cummins et al*., 2005]. Although PDO and AMO are indices for signals with a longer period than the timespan of this reconstruction, they were chosen because they are well known and still serve to show reconstruction accuracy in critical regions, albeit on shorter time scales.

2.5. Reconstruction Assumptions

Given that the specific purpose of this work is to compare EOF and CSEOF reconstruction methods in an idealized setting and not necessarily to create the most realistic reconstructions possible, a number of assumptions have been made for clarity and ease of calculation. For instance, a weighting scheme to account for areas with higher densities of tide gauges is not applied in the reconstruction process. Additionally, it is assumed that the synthetic tide gauges behave similarly to actual tide gauges with respect to variability in the open ocean. Because synthetic tide gauges are at distances of around 30 km from the actual coast and come from the training data set, our assumption is debatable. For comparison purposes, however, synthetic tide gauges sampled in this manner are assumed to be realistic enough for evaluation of the two techniques. Similarly, this process differs from true sea level reconstruction in that the global data set training period spans the entire tide gauge period. This would defeat the purpose of creating a useable reconstruction, but in this case allows for validation of reconstructions with the calibration data set over the entire time period. For the purpose of comparison, all reconstructions are made with basis functions that contain 70% of the training data set variance, with the exception of those discussed in section 6. Objective methods of determining the number of modes to retain while avoiding overfitting do exist (*CW2004*; *H2011*) but were not considered in the present work.

3. Tide Gauge Distribution

The number and distribution of useful tide gauges has varied over the past century (Figure 2), beginning with most of the gauges in the northern hemisphere, especially around Europe, and eventually taking on a more global distribution, including stations located on islands within ocean basins. The role that available tide gauges play on reconstruction quality is difficult to quantify with published reconstructions because of the lack of global data with which to compare prior to the calibration period. *Christiansen et al*. [2010] looked at the effect of tide gauge number on GMSL and found that varying the number of synthetic tide gauges from 20 to 200 improved the reconstructions only slightly. Here reconstructions are created using both methods, CSEOF and EOF, by fitting to tide gauge distributions from each decade over the past century. Figure 3 shows 20 year trend patterns from reconstructions with three different tide gauge

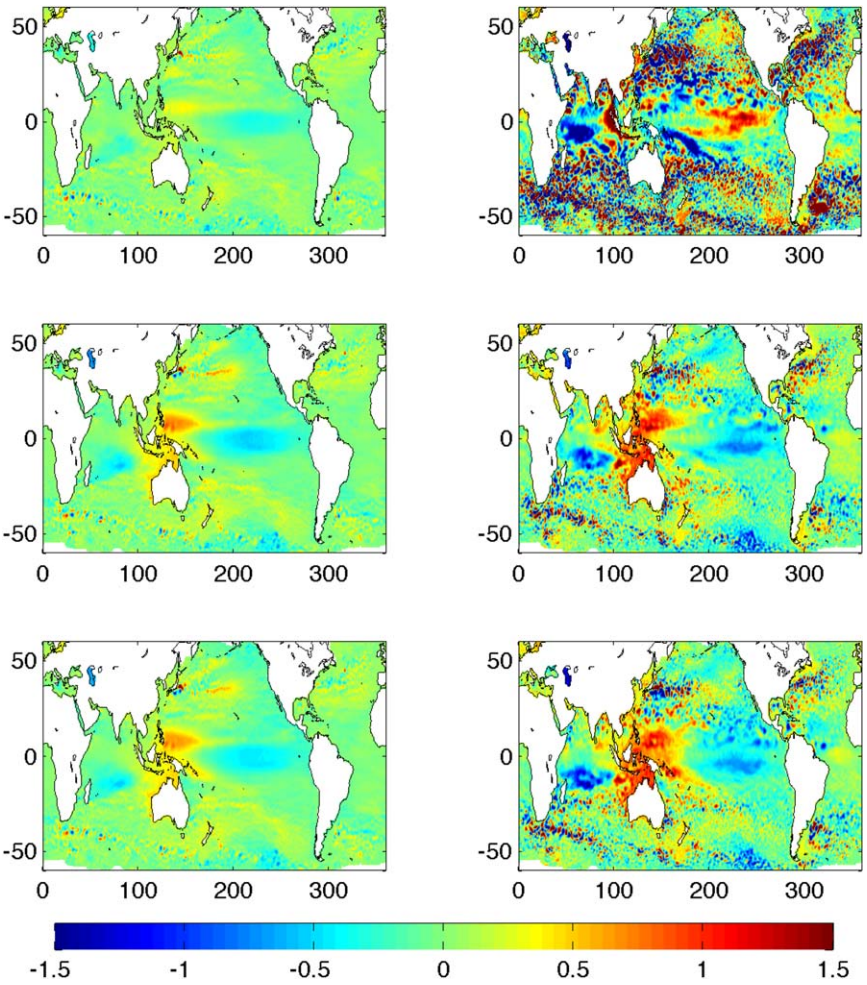

Figure 3. (left column) CSEOF reconstruction trend patterns and (right column) EOF reconstruction trend patterns calculated with synthetic tide gauge distribution from the (top row) 1930s, (middle row) 1970s, and all (bottom row) available tide gauges. All units in cm/yr.

distributions: the 1930s, the 1970s, and all available tide gauges. For simplicity, these will be referred to as CR30, CR70, and CRAA, for the CSEOF reconstructions, and ER30, ER70, and ERAA for the EOF reconstructions.

The left column in Figure 3 shows the regional trends in the CSEOF reconstructions as a function of synthetic tide gauge availability. It can be seen that with CR30, the trends have lower amplitude compared to CR70 and CRAA, although a similar pattern remains. This is most likely due to a lack of in situ measurements where regional trends are most prominent, such as the equatorial Pacific, during that time period. CR70 and CRAA are very similar to each other, with slightly lower amplitude in CRAA. When comparing this trend pattern with that of the training data (Figure 1), there is strong agreement with the exception of the southern tropics in the Indian Ocean. It should also be noted that the CSEOF reconstructions, in general, tend to slightly underestimate the regional trend, regardless of the tide gauge distribution.

The right column of Figure 3 shows the same trend patterns for the EOF reconstruction method. In general, these trend maps show much more stochastic signal in high latitudes, generally associated with over fitting. ER30 has very little spatial agreement with ER70 or ERAA. The latter two reconstructions agree in terms of general sea level trend patterns in the tropics (see Figure 1), but show much higher trend in the northern Indian Ocean and at the Indonesian throughflow region, and a negative trend in the southern tropical Indian Ocean. A plausible explanation is the lack of sufficient tide gauge representation in the Indian Ocean.

Although secular trends in GMSL were not considered in this work, interannual to decadal variability in GMSL has become a favored area of research [*Chambers et al*., 2012; *Hamlington et al*., 2013].Figure 4 shows

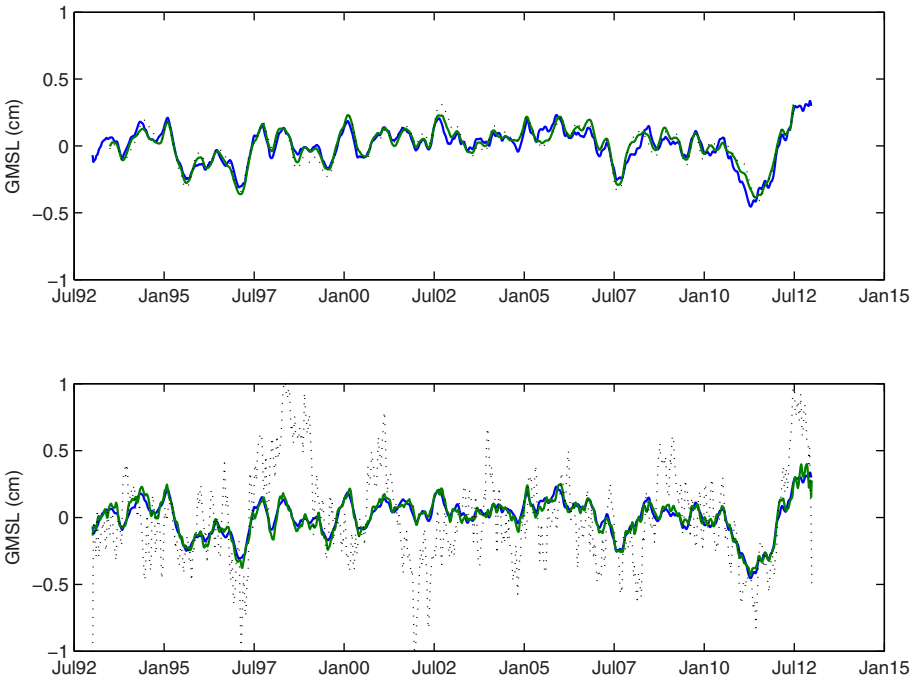

Figure 4. Detrended GMSL from AVISO (blue line) data compared to GMSL from (top) CSEOF reconstruction and (bottom) EOF reconstruction. Reconstructions with all tide gauge records are depicted by solid green lines, while reconstructions with 1930s tide gauge records are depicted by dotted lines. Note: all GMSL data have been smoothed by a 3 month moving average for clarity.

a GMSL comparison with the detrended training data and reconstructions calculated using all available and the 1930s tide gauge distributions. For clearer representation, all weekly data used in Figure 4 was smoothed by applying a 3 month moving window.

The CSEOF reconstructions agree well with the AVISO GMSL, both in phase and in amplitude. Note that using the lower quality CR30 does increase the amplitude of the GMSL variability slightly. Overall, the average GMSL amplitude from CR30 is 2% lower than that of the training data, while the average amplitude using CRAA is 9% below the training GMSL. There is no discernable difference between CR70 and CRAA when considering GMSL variability. The correlations associated with the training data set and CR30, CR70, and CRAA are 0.83, 0.88, and 0.89, respectively. Although there is slight dropoff in correlation from the limited tide gauge data set, these correlations are sufficiently high using sampling from the beginning of the century to suggest that a user could be confident in GMSL derived from a CSEOF reconstruction throughout the 20th century.

Table 1 also shows the correlation between various ocean indices calculated from the CSEOF reconstructions and the indices calculated from the AVISO training data. This further emphasizes the lack of dependence the CSEOF reconstruction method has on tide gauge distribution. With even a significant dropoff in the number of tide gauges, such as going from the complete tide gauge distribution to the 1900s distribution, GMSL correlation decreases by less than 13%. In fact, the average decrease in index correlation from the reconstruction where all available tide gauges are used to the reconstruction where the 1900s tide gauge distribution is used is only 6.4%.

The EOF reconstruction method overestimates GMSL under all tide gauge scenarios, which is in agreement with *Christiansen et al*. [2010]. When considering ER30, the amplitude overestimation is extreme, nearly 500% on average, as opposed to 30% with ERAA. Based on results by *Calafat et al*. [2014] that found that using an observational error of 2 cm and a limited number of EOF modes, and results from *Christiansen et al*. [2010] who also attribute overestimation in part to too many higher-order EOFs, using a higher observational error with less reconstructed EOF modes would likely curb this overestimation. The correlations associated with the training data set GMSL and that from ER30, ER70, and ERAA are 0.20, 0.66, and 0.72, respectively. Table 2 is identical to Table 1 but is for the EOF reconstructions. EOF reconstructions show a

Table 1. Correlation Between Parameters Calculated From AVISO Training Data Set and Parameters Calculated From Various CSEOF Reconstructions

	GMSL	PDO	AMO	Nino 3	Nino 4
1900s (61 tide gauges)	0.773	0.656	0.850	0.927	0.907
1920s (76 tide gauges)	0.812	0.654	0.868	0.936	0.923
1940s (108 tide gauges)	0.872	0.685	0.902	0.975	0.954
1960s (243 tide gauges)	0.878	0.678	0.907	0.982	0.962
1980s (292 tide gauges)	0.877	0.660	0.912	0.977	0.967
2000s (277 tide gauges)	0.888	0.644	0.911	0.970	0.965
All gauges (412 tide gauges, 70% variance explained with 11 modes)	0.886	0.651	0.911	0.979	0.967
All gauges with high-frequency signal	0.886	0.658	0.910	0.977	0.967
All gauges (90% variance explained with 16 modes)	0.953	0.655	0.958	0.984	0.980
All gauges (90% variance) with high-frequency signal	0.953	0.666	0.957	0.982	0.980

significant degradation of signal when working with limited tide gauge distributions. The average decrease in correlation across all indices from the reconstruction with complete tide gauge data set to the reconstruction with the 1900s distribution is 88.0%. This analysis suggests that the accuracy of an EOF reconstruction could be significantly degraded using historical tide gauge distributions before 1950, and care should be taken with time-varying tide gauge distributions when reconstructing sea level.

When considering reconstructions with all available tide gauges, additional observations from Tables 1 and 2 can be made. Variability in the Niño regions is captured very well using both methods of reconstruction. Signals on time scales similar to the PDO are more elusive with both reconstruction methods, and GMSL and AMO are in the reconstructions, but not as well reproduced as the stronger equatorial (Niño) signals.

4. High-Frequency Signal in the Tide Gauge Records

To investigate how more realistic tide gauge measurements would affect reconstruction quality, actual tide gauge data were processed as described in Section 2.2 to estimate a realistic high-frequency signal that could be added to the synthetic tide gauge time series. Reconstructions were created with the synthetic tide gauge data set including this real, high-frequency signal to be compared to those reconstructions with the complete synthetic tide gauge data set and the training data set. In addition to trend maps, correlation between the reconstructions and training data, and relative amplitude are calculated at each grid point. As in *Christiansen et al.* [2010], the relative amplitude is calculated as $(\sigma_{rec} - \sigma_{AVISO})/\sigma_{AVISO}$, where σ_{rec} and σ_{AVISO} are the standard deviations of each grid point in the reconstruction and AVISO data sets, respectively. Ideal relative amplitude has a value of 0, with negative values showing underestimation by the reconstruction and positive values showing overestimation.

Figure 5 shows trend, correlation, and relative amplitude maps for CSEOF reconstructions created from all available tide gauges with and without added signal. There is no discernable difference in the maps when adding high-frequency signal to the tide gauge data sets. Table 1 shows that the correlation associated with the PDO, AMO and Nino3 changes only slightly with the more realistic tide gauges. The lack of sensitivity with additional higher-frequency signal in the CSEOF reconstruction is due to the use of tide gauge data at multiple (52) time steps when computing the amplitude of CSEOF loading vectors, which effectively smooths the more stochastic signal within the temporal window during the fitting process. Figure 5 shows

Table 2. Correlation Between Parameters Calculated From AVISO Training Data Set and Parameters Calculated From Various EOF Reconstructions

	GMSL	PDO	AMO	Nino 3	Nino 4
1900s (61 tide gauges)	0.112	0.018	0.095	0.226	0.042
1920s (76 tide gauges)	0.077	0.131	0.172	0.150	0.036
1940s (108 tide gauges)	0.059	0.019	0.138	0.115	0.045
1960s (243 tide gauges)	0.642	0.449	0.663	0.925	0.896
1980s (292 tide gauges)	0.710	0.498	0.729	0.947	0.958
2000s (277 tide gauges)	0.666	0.480	0.722	0.898	0.909
All gauges (412 tide gauges, 70% variance explained with 108 modes)	0.716	0.519	0.765	0.950	0.970
All gauges with high-frequency signal	0.689	0.467	0.701	0.935	0.953
All gauges (90% variance explained with 237 modes)	0.811	0.534	0.817	0.953	0.973
All gauges (90% variance) with high-frequency signal	0.684	0.418	0.556	0.887	0.943

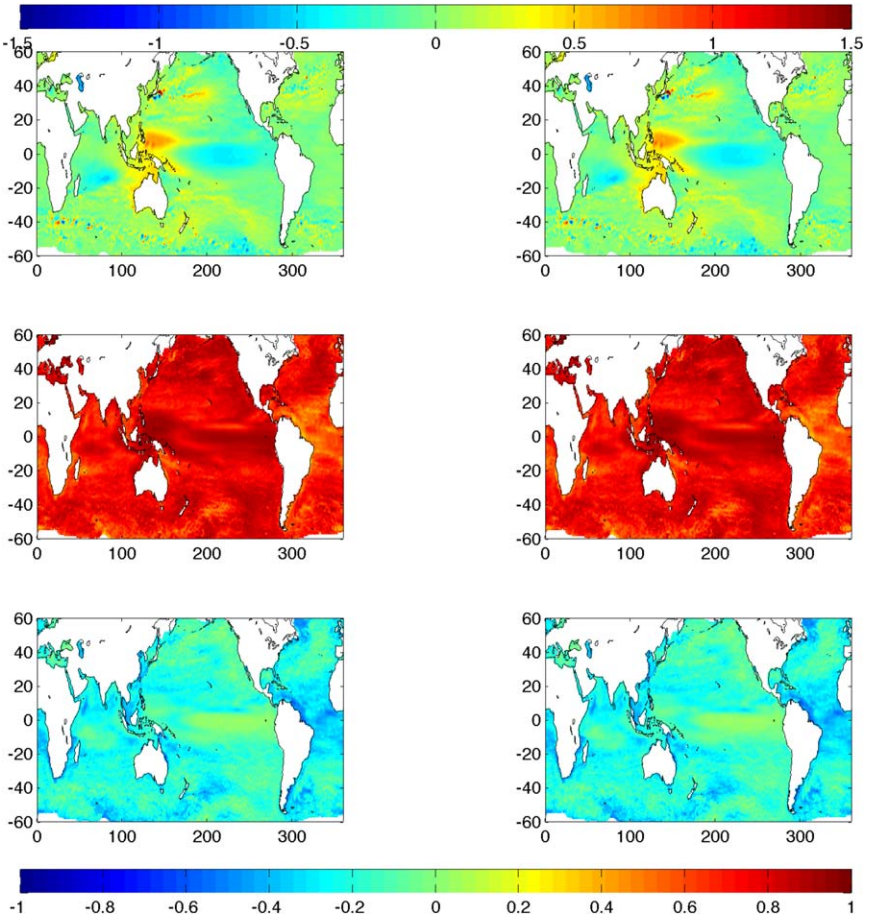

Figure 5. (left column) CSEOF reconstruction and (right column) CSEOF Reconstruction with added high-frequency tide gauge signal (top row) trend maps, (middle row) correlations, and (bottom row) relative amplitudes. Note: the top colorbar (in cm/yr) is associated with the top row, while the bottom colorbar is associated with the middle and bottom rows; ideal relative amplitude has a value of 0.

that correlation is generally quite high, particularly as the equatorial Pacific. There are certain areas, such as the Central Atlantic where agreement is not as good. This is most likely due to lack of sufficient in situ representation in that region. As for the relative amplitude, it should be noted the reconstructions are very close to the satellite altimetry data in amplitude or slightly underestimate it with the exception of the equatorial central to western Pacific; this is in agreement with the GMSL results from Figure 4.

A similar plot for the EOF method of sea level (Figure 6) shows that trend maps computed from EOF reconstructions with and without high-frequency signal agree quite well. However, the correlation decreases and relative amplitude is overestimated significantly over the tropics and midlatitude regions. These results are consistent with or without added high-frequency signal. Table 2 shows that the correlation of all indices decreases when adding realistic signal to the ideal simulated tide gauge data. Although the correlation changes are less than 0.07, they are an order of magnitude larger than that seen in the CSEOF reconstructions. Similar to the CSEOF correlation and amplitude maps, the EOF maps show that the reconstructions agree with AVISO well in the Equatorial Pacific. However, outside of that region, correlations are generally much lower than seen with the CSEOF method. Also, the relative amplitude shows that outside the Pacific and high-latitude regions, the reconstructions generally overestimate sea level signals. Again, this agrees with what was seen in the GMSL analysis (Figure 4).

GMSL was calculated using reconstructions from both basis function methods with and without the addition of high-frequency signal to the tide gauges. This is plotted along side the AVISO GMSL with the detrended, seasonal signal removed (Figure 7). The GMSLs from the CSEOF reconstructions agree very well with the GMSL from AVISO, and adding high-frequency tide gauge signal does not alter the reconstruction in any visible way. Overall, it increases the average amplitude underestimation by 1% to a total of 9% below

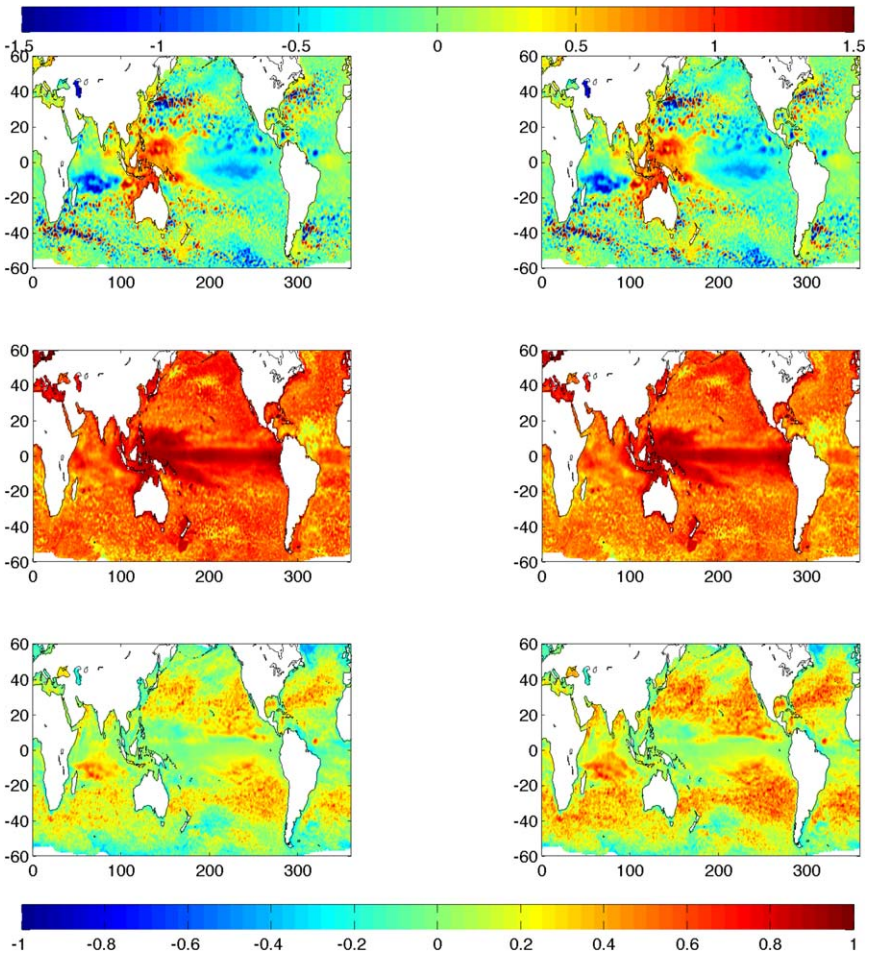

Figure 6. (left column) EOF reconstruction and (right column) EOF reconstruction with added high-frequency tide gauge signal (top row) trend maps, (middle row) correlations, and (bottom row) relative amplitudes.

the training data GMSL magnitude. This underestimation may be natural since only a small number of CSEOF modes are used for reconstruction. Adding more modes may decrease amplitude underestimation. The EOF GMSL signal has more stochasticity than the training data GMSL. Note that adding high-frequency signal to the synthetic tide gauges increases the signal overestimation slightly (from 30% to 35%), although not nearly as much as using sparse tide gauge distributions (Figure 4). Comparing the relative amplitude maps indicates that the CSEOF (EOF) method tends to underestimate (overestimate) the true signal. To confirm these results, this analysis was also performed using random white noise with a standard deviation of 2.8 cm. Although the effects were smaller, the findings were confirmed.

5. Selected Variance

Before creating any reconstruction, the question of how much variance should be kept in the basis functions must be answered. *CW2004* kept over 80% (using 20 EOF modes) not including the seasonal cycle in their $1^\circ \times 1^\circ$ monthly reconstruction, and *H2011* kept over 95% (using 19 CSEOF modes) including the seasonal cycle with a $0.5^\circ \times 0.5^\circ$ weekly reconstruction, shown in Figure 1. In order to create the reconstructions with 70% of the original variance, 108 EOF modes were required, whereas only 11 CSEOF modes were needed. For comparison, reconstructions were also created using 90% of the original variance. In this case, 237 EOF modes and 16 CSEOF modes were required. This highlights that CSEOFs are able to capture more variability with fewer modes, agreeing with results found in *H2011*.

Figure 8 shows the trend patterns associated with the reconstructions created using the previously explained tide gauge distributions and basis functions containing 90% variance. When comparing to Figure

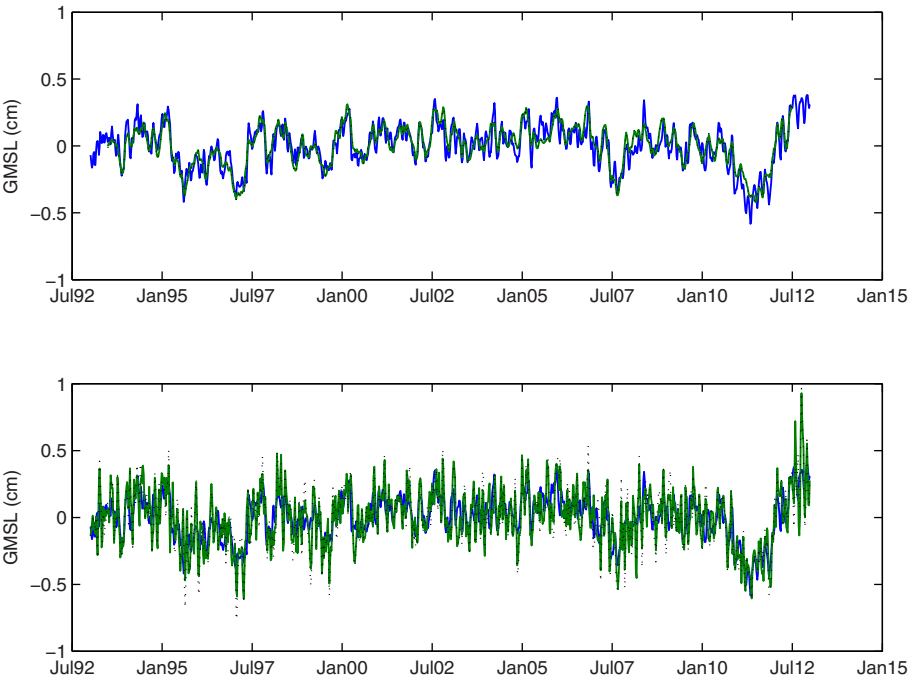

Figure 7. Detrended GMSL from AVISO (blue line) data compared to GMSL from (top) CSEOF reconstruction and (bottom) EOF reconstruction. Reconstructions with purely synthetic tide gauge records are depicted by solid green lines, while those with added high-frequency signal are depicted by dotted lines.

3, the CSEOF trend maps are essentially unchanged regardless of whether 70% or 90% of the original variance is used. Correlations with the ocean indices calculated from the training data (Table 1) show very slight improvements (∼1%) for the PDO and the Niño indices, while the GMSL and AMO correlation improved by 8% and 5%, respectively, when increasing the variance explained from 70% to 90. These results are for all available tide gauges and valid using both the standard and noisy tide gauge data sets. These increased correlations are due to more accurate reconstruction in areas with less dominant variability, such as the North Atlantic.

Similar observations can be made with the EOF reconstructions. In this case, it can be seen that the trend maps differ significantly when using 70% or 90% of the variance. When comparing Figure 8 to Figure 3, some key observations about using more variance can be inferred: for ER30, the amount of noise is similar but some of the dominant equatorial features are lost; for ER70, the trend map becomes much noisier, including the main equatorial features; for ERAA, the amount of noise increases moderately and the features change slightly. In all cases, the peak amplitudes increase on top of the existing overestimation. This suggests that too much variability was kept in the basis functions, causing over fitting of the synthetic tide gauge records.

When comparing the index correlations from the 70% variance, nonnoisy, full tide gauge reconstruction in Table 2 to similar correlations with a 90% variance reconstruction, conclusions similar to the CSEOF conclusions can be made. With more variance, correlations of PDO and Niño indices increase by 3% and less than 1%, respectively. GMSL correlation increases by 13%, and AMO correlation increases by 7%. However, when considering noisy tide gauges, the reconstruction with more variance has less correlation with all of the chosen indices. GMSL, PDO, AMO, Niño3, and Niño4 correlations decrease by 5%, 19%, 27%, 7%, and 3%, respectively, when reconstructing with 90% of the total variance as opposed to 70%.

6. Conclusions and Discussion

Sea level reconstructions have proven useful in a wide variety of scientific applications, from studying GMSL trends to examining modulations of the annual cycle. It has, however, proven difficult to verify the accuracy of reconstructions prior to the era of satellite altimetry. One way to verify reconstruction methods is to reconstruct a known data set, such as the global altimetry data set in an idealized setting. This paper

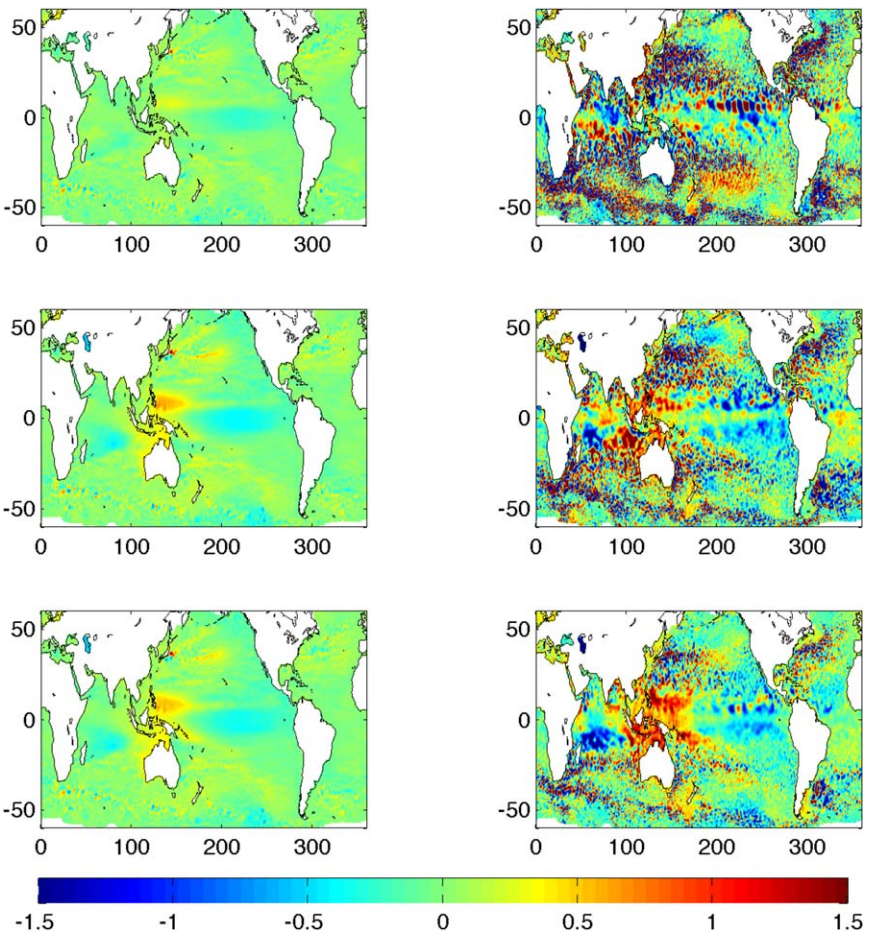

Figure 8. Similar to Figure 3 with 90% of the decomposed variance remaining in the reconstructions. Colorbar units are cm/yr.

compares two methods of calculating basis functions for sea level reconstructions. Both EOF and CSEOF decomposition techniques are used to calculate basis functions from a 20 year AVISO satellite altimetry SSH data set. These basis functions are then fit to a variety of synthetic tide gauge time series to create sea level reconstructions. The direct comparison between both reconstruction techniques gives important insight into how the methods vary in a controlled experiment. While not using real tide gauges and therefore lacking realism, similar conclusions with regards to overfitting and the ability to capture climate variability can be made with regards to the publicly available reconstructions. The conclusions derived herein also provide important guidelines for both creating and using sea level reconstructions by highlighting some of the benefits and deficiencies of each reconstruction technique.

For limited tide gauge distributions, such as those found in the early 20th century, the CSEOF reconstruction method is affected far less than the EOF reconstruction method. Overall, the CSEOF reconstruction accurately reproduces known signals regardless of significant limitations in the tide gauge data set. However, this method slightly underestimates regional trend amplitudes and global variability. This is due to the use of a small number of CSEOF modes, along with under representation of in situ measurements in areas with the largest trends. The superior ability to maintain trend patterns and regional variability stems from the temporal connectivity of the LVs attributed to the nested period. This allows CSEOF reconstructions to separate ocean signals, such as wave oscillations, from regional trends, even with sparse tide gauge locations. Likewise, the lack of effect of noisy tide gauge data on the CSEOF reconstruction stems from a natural temporal averaging created by the windowing of data over the nested period. Similarly, this limits the likelihood of over fitting the data, despite reconstructing more of original data set variance and using noisy tide gauges.

The quality of EOF reconstructions decreases far more with limited tide gauge data sets. When considering trend patterns with historical tide gauge distributions, the most limited distributions cause primary features to be lost, noisy spatial patterns to be created, and amplitudes to be overestimated. Trying to reproduce such high temporal and spatial resolution with fixed spatial patterns causes overemphasis of certain modes, causing vastly overestimated amplitudes in GMSL and in regions without dominant signals (nonequatorial). Additionally, the lack of ability to separate moving periodic signals is portrayed in the reduced correlations between reconstruction calculated and training data set calculated oceanic indices. Care must be taken when trying to reproduce too much of the original variance with EOF reconstructions, or noise can be reconstructed thereby reducing the quality. Conversely, it is reasonable to reduce the number of EOF modes as the number of tide gauge records decrease to avoid over fitting [*Church and White*, 2011], causing the reconstruction to explain less overall variance as it extends back through time. This issue can be avoided altogether with CSEOF reconstruction.

Although these results yield great insight into both methods of reconstruction, many assumptions were made, which could be investigated further. For instance, as discussed in *Calafat et al*. [2014], synthetic tide gauges are not necessarily representative of the relationship between real tide gauges and the open ocean. While the focus here was on a direct comparison between techniques and not on deficiencies of reconstructions in general, similar analysis could be done in the future using real tide gauge data and perhaps provide additional information on how best to complete reconstructions. It is doubtful that these results would be as extreme with a calibration data set of less spatial and temporal resolution. The EOF method could perform better using monthly data or a more sparsely gridded calibration data set because there would be less "noisy" signal to separate. This analysis assumed a constant tide gauge distribution over the entire reconstruction time period, when in reality the number of tide gauges changes frequently. It is unknown whether mimicking the time-varying tide gauge distribution would change these results but this could be investigated in the future. Lastly, the trend patterns over this relatively short period are largely influenced by ENSO and other modes of variability, which are captured well with the CSEOF decomposition. Over a longer time period, such as one seen with a published reconstruction (60–100 years), the trend processes are more complex and may not be captured as well in the decomposition, and thus one would have less confidence that the reconstructed trends would be accurate.

Based on the experiment above, it seems that calculating basis functions through CSEOF decomposition, as opposed to EOF decomposition, allows for more robust sea level reconstructions throughout this controlled experiment. This method was found to better reconstruct regional trend patterns, common oceanic indices, and GMSL variability with nearly all synthetic tide gauge distributions, with the addition of high-frequency tide gauge signal, and with different amounts of reconstructed variance.

Acknowledgments

M.W.S., B.D.H., and R.R.L. acknowledge support from NASA ROSES grant NNX13AH05G. K.-Y.K. acknowledges support by the project entitled "Ocean Climate Change: Analysis, Projections, Adaptation (OCCAPA)" funded by the Ministry of Land, Transport, and Maritime Affairs, Korea. The altimeter products used in this study were produced by Ssalto/Duacs and distributed by AVISO, with support from the Centre National d'Etudes Spatiales (CNES). Tide gauge locations were obtained from Permanent Service for Mean Sea Level (PSMSL), 2014, "Tide Gauge Data," retrieved August 2010 from http://www.psmsl.org/data/obtaining/.

References

Berge-Nguyen, M., A. Cazenave, A. Lombard, W. Llovel, J. Viarre, and J. F. Cretaux (2008), Reconstruction of past decades sea level using thermosteric sea level, tide gauge, satellite altimetry and ocean reanalysis data, *Global Planet. Change*, *62*, 1–13, doi:10.1016/j.gloplacha.2007.11.007.

Calafat, F. M., D. P. Chambers, and M. N. Tsimplis (2014), On the ability of global sea level reconstructions to determine trends and variability, *J. Geophys. Res. Oceans*, *119*, 1572–1592, doi:10.1002/2013JC009298.

Chambers, D. P., C. A. Melhaff, T. J. Urban, D. Fuji, and R. S. Nerem (2002), Low-frequency variations in global mean sea level: 1950–2000, *J. Geophys. Res.*, *107*(C4), 3026, doi:10.1029/2001JC001089.

Chambers, D. P., M. A. Merrifield, and R. S. Nerem (2012), Is there a 60-year oscillation in global mean sea level, *Geophys. Res. Lett.*, *39*, L18607, doi:10.1029/2012GL052885.

Christiansen, B., T. Schmith, and P. Thejll (2010), A surrogate ensemble study of sea level reconstructions, *J. Clim.*, *23*:4306–4326, doi:10.1175/2010JCLI3014.1.

Church, J. A., and N. J. White (2011), Sea-level rise from the late 19th to the early 21st century, *Surv. Geophys.*, *32*(4), 585–602, doi:10.1007/s10712-011-9119-1.

Church, J. A., N. J. White, R. Coleman, K. Layback, and J. X. Mitrovica (2004), Estimates of the regional distribution of sea level rise over the 1950–2000 period, *J. Clim.*, *17*, 2609–2625, doi:10.1175/1520-0442(2004)017%3C2609:EOTRDO%3E2.0.CO;2.

Cummins, P., G. Lagerloef, and G. Mitchum (2005), A regional index of northeast Pacific variability based on satellite altimeter data, *Geophys. Res. Lett.*, *32*, L17607, doi:10.1029/2005GL023642.

Hamlington, B. D., R. R. Leben, R. S. Nerem, W. Han, and K.-Y. Kim (2011), Reconstructing sea level using cyclostationary empirical orthogonal functions, *J. Geophys. Res.*, *116*, C12015, doi:10.1029/2011JC007529.

Hamlington, B. D., R. R. Leben, and K.-Y. Kim. (2012), Improving sea level reconstructions using non-sea level measurements, *J. Geophys. Res.*, *117*, C10025, doi:10.1029/2012JC008277.

Hamlington, B. D., R. R. Leben, M. W. Strassburg, R. S. Nerem, and K.-Y. Kim (2013), Contribution of the Pacific Decadal Oscillation to global mean sea level trends, *Geophys. Res. Lett.*, *40*, 5171–5175, doi:10.1002/grl.50950.

Kaplan, A. M., M. A. Cane, Y. Kushnir, A. C. Clement, M. B. Blumenthal, and B. Rajagopalan (1998), Analyses of global sea surface temperature 1856–1991, *J. Geophys. Res.*, *103*, 18,567–17,589, doi:10.1029/97JC01736.

Kerr, R. A. (2000), A North Atlantic climate pacemaker for the centuries, *Science*, *288*, 1984–1985, doi:10.1126/science.288.5473.1984.

Kim, K.-Y., and G. R. North (1997), EOFs of harmonizable cyclostationary processes, *J. Atmos. Sci.*, *54*, 2416–2427, doi:10.1175/1520-0469(1997)054%3C2416:EOHCP%3E2.0.CO;2.

Kim, K.-Y., and Q. Wu (1999), A comparison of study of EOF techniques: Analysis of nonstationary data with periodic statistics, *J. Clim.*, *12*, 185–199, doi:10.1175/1520-0442-12.1.185.

Kim, K.-Y., G. R. North, and J. Huang (1996), EOFs of one-dimensional cyclostationary time series: Computations, examples, and stochastic modelling, *J. Atmos. Sci.*, *53*, 1007–1017, doi:10.1175/1520-0469(1996)053<1007:EOODCT>2.0.CO;2.

Le Traon, P.-Y., F. Nadal, and N. Ducet (1998), An improved mapping method of multi-satellite altimeter data, *J. Atmos. Oceanic Technol.*, *15*, 522–534, doi:10.1175/1520-0426(1998)015<0522:AIMMOM>2.0.CO;2.

Llovel, W., A. Cazenave, P. Rogel, A. Lombard, and M. B. Nguyen (2009), Two- dimensional reconstruction of past sea level (1950–2003) from tide gauge data and an Ocean General Circulation Model, *Clim. Past*, *5*, 217–227, doi:10.5194/cp- 5-217-2009.

Meyssignac, B., M. Becker, W. Llovel, and A. Cazenave (2012), Assessment of two dimensional past sea level reconstructions over 1950–2009 based on tide-gauge data and different input sea level grids, *Surv. Geophys.*, *33*(5), 945–972, doi:10.1007/s10712-011-9171-x.

Ray, R., and B. Douglas (2011), Experiments in reconstructing twentieth-century sea 1048 levels, *Prog. Oceanogr.*, *91*, 496–515, doi:10.1016/j.pocean.2011.07.021.

Smith, T. M., and R. W. Reynolds (2004), Improved extended reconstruction of SST (1854–1997), *J. Clim.*, *17*, 2466–2477, doi:10.1175/1520-0442(2004)017%3C2466:IEROS%3E2.0.CO;2.

Smith, T. M., R. W. Reynolds, R. E. Livezey, and D. C. Stokes (1996), Reconstruction of historical sea surface temperatures using empirical orthogonal functions, *J. Clim.*, *9*, 1403–1420, doi:10.1175/1520-0442(1996)009<1403:ROHSST>2.0.CO;2.

Stenseth, N. C., G. Ottersen, J. W. Hurrell, A. Mysterud, M. Lima, K. S. Chan, N. G. Yoccoz, and B. Ådlandsvik (2003), Studying climate effects on ecology through the use of climate indices: The North Atlantic Oscillation, El Nino Southern Oscillation and beyond, *Proc. R. Soc. London, Ser. B*, *270*, 2087–2096, doi:10.1098/rspb.2003.2415.

van Onselen, K. I. (2000), The influence of data quality on the detectability of sea-level height variations, PhD thesis, in NCG Publications on Geodesy, vol. 49, pp. 67–69, TU Delft, Delft, Netherlands.

Yeo, S. R., and K.-Y. Kim (2013), Global warming, low-frequency variability, and biennial oscillation: An attempt to understand the physical mechanisms driving major ENSO events, *Clim. Dyn.*, doi:10.1007/s00382-013-1862-1.